

# Processing of Alumina-Niobium Interfaces via Liquid-Film-Assisted Joining

*The average strength of bonds between niobium and polished alumina substrates increased with the introduction of copper film interlayers*

BY J. T. McKEOWN, J. D. SUGAR, R. GRONSKY, AND A. M. GLAESER

**ABSTRACT.** Alumina-niobium interfaces were fabricated at 1400°C via solid-state diffusion brazing of a 127- $\mu\text{m}$ -thick niobium foil between alumina blocks. Prior to brazing, some of the alumina mating surfaces, both polished and unpolished, were evaporation-coated with copper films  $\approx 1.4$ ,  $\approx 3.0$ , and  $\approx 5.5$   $\mu\text{m}$  thick to induce liquid-film-assisted joining at the brazing temperature. The effects of copper film thickness and surface roughness on fracture characteristics and ceramic-metal interfacial microstructure were investigated by room-temperature four-point bend tests, optical microscopy, profilometry, and atomic force microscopy. The average strength of bonds between niobium and polished alumina substrates increased with the introduction of copper film interlayers, and the scatter in strength tended to decrease, with an optimum combination of strength and Weibull modulus arising for a copper film thickness of 3.0  $\mu\text{m}$ . The strength characteristics of niobium bonded to unpolished alumina substrates were also improved by liquid-film-assisted joining, but were unaffected by the thickness of the copper interlayers.

## Introduction

Bonded ceramic-metal interfaces play a vital role in modern materials applications. Precise control of interfacial microstructure through processing is therefore essential, and the development of processing-microstructure-properties correlations is of sound fundamental value. Among the more widely studied ceramic-metal systems is alumina-niobium, which, due to closely matched thermal expansion coefficients, results in bonded interfaces that are virtually free of thermal stresses. Considerable research has previously been conducted on the mechanical properties and interfacial characterization of this system

*J. T. McKEOWN, J. D. SUGAR, R. GRONSKY, and A. M. GLAESER are with the Department of Materials Science & Engineering, University of California, and Division of Materials Science, Lawrence Berkeley National Laboratory, Berkeley, Calif.*

(Refs. 1–9). Niobium and alumina are also chemically compatible, resulting in interfaces with no chemical reaction layer when bonded in vacuum (Refs. 2, 7, 10).

In the present study, alumina was joined using copper/niobium/copper interlayers via liquid-film-assisted joining (LFAJ). The LFAJ approach to joining ceramics employs a multilayer metallic interlayer composed of two thin cladding layers of a low-melting-point metal (copper) and a thick core of a high-melting-point or refractory metal (niobium) between sections of the ceramic to be joined (alumina). Copper was chosen as the liquid former because of its low melting point, ease of deposition, previous research on the joining of copper and alumina via diffusion brazing and partial transient liquid phase (PTLP) bonding, previous fracture studies of alumina-copper interfaces, and the past success of PTLTP bonding with copper (see Ref. 7 and references therein). The joining temperature is above the melting point of copper but below that of niobium; consequently, during the initial stages of bonding, a thin, copper-rich liquid film develops between the alumina and niobium, resulting in heterophase liquid-phase sintering. Redistribution of this liquid layer fills voids at the interface and provides a path for the rapid diffusion of niobium, which, in turn, accelerates contact formation between the alumina and niobium. Fractography of the interfaces indicates that the liquid copper film results in more extensive alumina-niobium contact compared to solid-state diffusion brazing, and concomitantly improved strength (Refs. 11, 12). The copper film becomes discontinuous, and upon

cooling from the bonding temperature, discrete particles of copper remain at the interface due to the limited solubility and slow diffusion of copper in niobium. Plastic deformation of the ductile copper particles increases the toughness of the interface (Ref. 13), and tearing of this ductile metal during fracture has been observed (Refs. 11, 12). The goal of this research was to explore the effects of selected processing conditions (copper film thickness, alumina surface finish) on the interfacial microstructure and mechanical properties of joined assemblies.

## Background

Extensive discussions of the alumina-niobium and sapphire-niobium systems can be found in the literature (Refs. 2, 4, 5, 8, 14–30) and prior publications (Refs. 7, 9, 11, 12). Copper-niobium is an attractive brazing system for joining alumina because there are no brittle intermediate phases, and at temperatures above the melting point of copper, the composition of the equilibrium liquid contains a few at.-% of niobium (Ref. 31), which has been shown to enhance the wetting of copper on alumina (Refs. 32–34).

Prior studies by Shalz et al. (Ref. 7) and Marks et al. (Ref. 11) have established that pressure and temperature can have an important influence on joint characteristics. At a fixed bonding temperature of 1150°C, increasing the applied load during vacuum bonding from 2.2 to 5.1 MPa increased the average strength in four-point bend tests from  $78 \pm 22$  to  $181 \pm 45$  MPa.<sup>1</sup> In both joints, failures occurred primarily along the alumina-niobium interface. At a fixed bonding pressure of 2.2 MPa, increasing the bonding temperature from 1150° to 1400°C increased the four-point bend strength from  $78 \pm 22$  to  $241 \pm 18$

## KEYWORDS

Alumina  
Niobium  
Diffusion Brazing  
Liquid-Film-Assisted Joining  
Copper Film  
Fracture Path  
Area Fracture of Contact

*1. The average strength represents the mean of the measured fracture strengths for a given set of joining conditions, not the median strength in a Weibull distribution. The error ranges represent  $\pm 1$  standard deviation of the measured strengths for a given set of joining conditions. These definitions are used throughout the paper.*

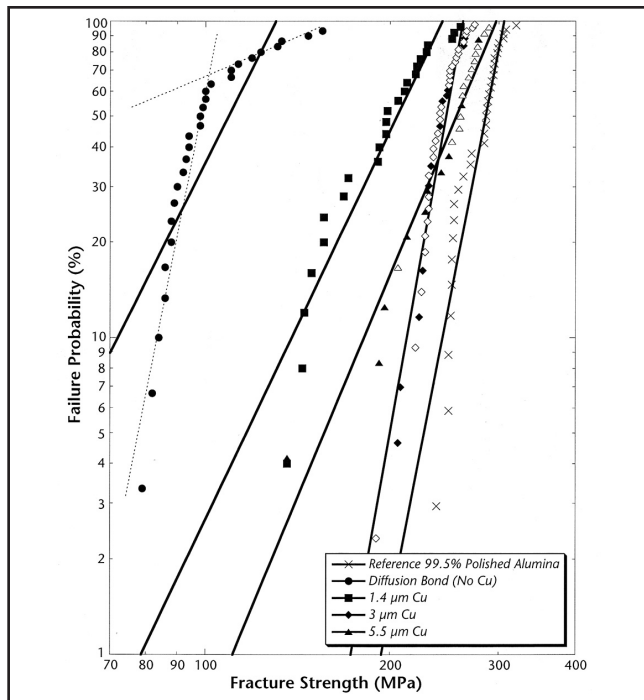


Fig. 1 — Failure probability vs. fracture strength for joints processed with polished  $\text{Al}_2\text{O}_3$  substrates. Filled symbols indicate failure along the  $\text{Al}_2\text{O}_3$ -Nb interface; open symbols indicate failure in the ceramic.

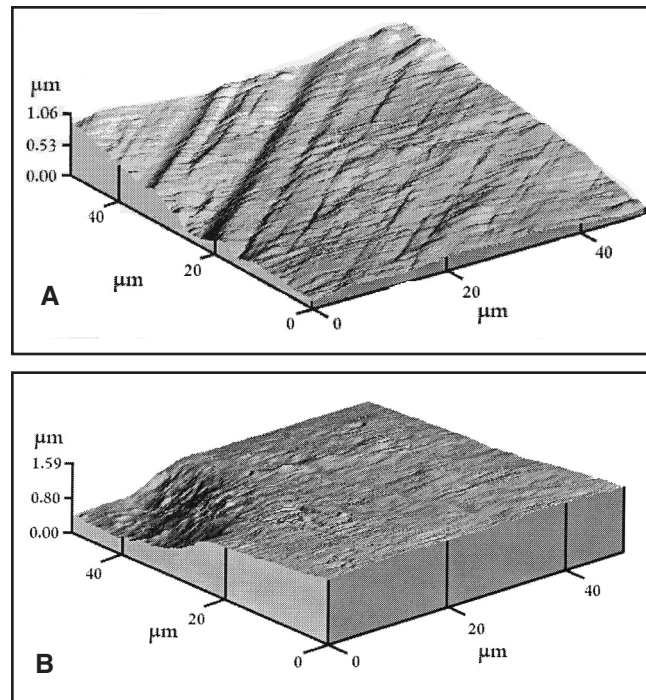


Fig. 2 — AFM images showing regions on the surfaces of (A) as-received Nb and (B) flattened Nb. Note the depression on the surface of the flattened Nb. The average roughness of the as-received and flattened Nb is, respectively, 107 and 97 nm.

MPa, and  $\approx 75\%$  of the samples failed in the ceramic. For samples processed at  $1400^\circ\text{C}$ , ceramic failures were also observed in high-temperature fracture tests up to  $1100^\circ\text{C}$ , suggesting the formation of a strong interface with potential for use at elevated temperature (Ref. 11).

In prior studies with copper/niobium/copper interlayers (Ref. 11), local variations in the copper film thickness were observed to affect strength characteristics. In two samples bonded under the same conditions ( $1150^\circ\text{C}$ , 2.2 MPa), the weaker sample had a copper thickness of  $3.8\ \mu\text{m}$ , while the stronger had a copper thickness of  $3.0\ \mu\text{m}$ . The (interfacial) fracture surfaces of the weaker samples were dominated by copper, while the stronger samples displayed more alumina- niobium contact. Local variations in copper thickness can cause spatial variations in the time required to initiate widespread alumina- niobium contact and the extent of ensuing alumina- niobium contact growth (Ref. 11). The kinetics of copper film breakup depends on the film thickness, and excessively thick films are expected to degrade joint properties.

Liu et al. (Ref. 35) examined the effects of a thin-film niobium interlayer on the fracture strength of sapphire-copper diffusion brazes. Niobium interlayers were deposited by e-beam evaporation onto the joining surfaces of the sapphire prior to diffusion brazing. The introduction of thin niobium films greatly improved the sap-

phire-copper bond strength. The fracture energies of sapphire- niobium-copper joints were significantly higher than sapphire-copper joints processed without a niobium interlayer. This was attributed to strong adhesion of niobium to alumina relative to that of copper to alumina combined with plastic deformation in the copper during fracture. A theoretical value for the work of adhesion of a pure sapphire- niobium interface is  $0.8\ \text{J/m}^2$  (Ref. 36), while an experimental value of  $1.63\ \text{J/m}^2$  was reported by Jilavi (Ref. 37) (as cited in Ref. 35). Experimental values for the work of adhesion for a sapphire-copper interface range from  $0.49$  to  $0.54\ \text{J/m}^2$  (Refs. 38, 39). The fracture energy is related to the work of adhesion by a power law (Ref. 27). Plastic deformation in sapphire-copper interfaces without a niobium interlayer is still possible, but the weaker bonding of copper to sapphire leads to brittle debonding along the interface and limited plastic deformation (Ref. 35).

Sugar et al. (Ref. 12) have also reported strength degradation in assemblies in which the copper film thickness was decreased sufficiently. This is attributed to an increase in the density of interfacial flaws when an inadequate amount of copper is available to fill irregularities and gaps between the two mating surfaces. Careful polishing and surface preparation should in principle reduce the severity of surface irregularities and thus reduce the amount of copper required to fill interfa-

cial gaps. An interplay between film thickness and surface preparation can be expected, with the potential emergence of an optimum film thickness and surface preparation combination.

Surface roughness will not only influence the size and spatial distribution of the gaps between mating surfaces, but can also have multiple additional and opposing effects on the strength of a ceramic-metal interface. A roughened surface can prevent ceramic-metal contact at the interface with large deviations from planarity leading to sharp, crack-like interfacial flaws. Deep scratches on a ceramic surface will not be completely filled by a nonwetting liquid metal, introducing near-interfacial flaws. Surface roughness will have an effect on the wettability of a liquid metal on a ceramic substrate. Increased roughness may also introduce near-surface damage and flaws, particularly in brittle materials. However, a rough interface can lead to an anchoring effect that promotes joining by mechanical interlocking at the interface (Refs. 40, 41). Together, these effects influence the mechanical properties of a joint. Relatively few studies have explored and quantified the effects of surface roughness on ultimate ceramic-metal joint properties.

Suganuma et al. (Ref. 40) investigated the effects of surface damage introduced by grinding on the properties of silicon nitride joints prepared with a pure aluminum braze. Brazing involved a 10 min

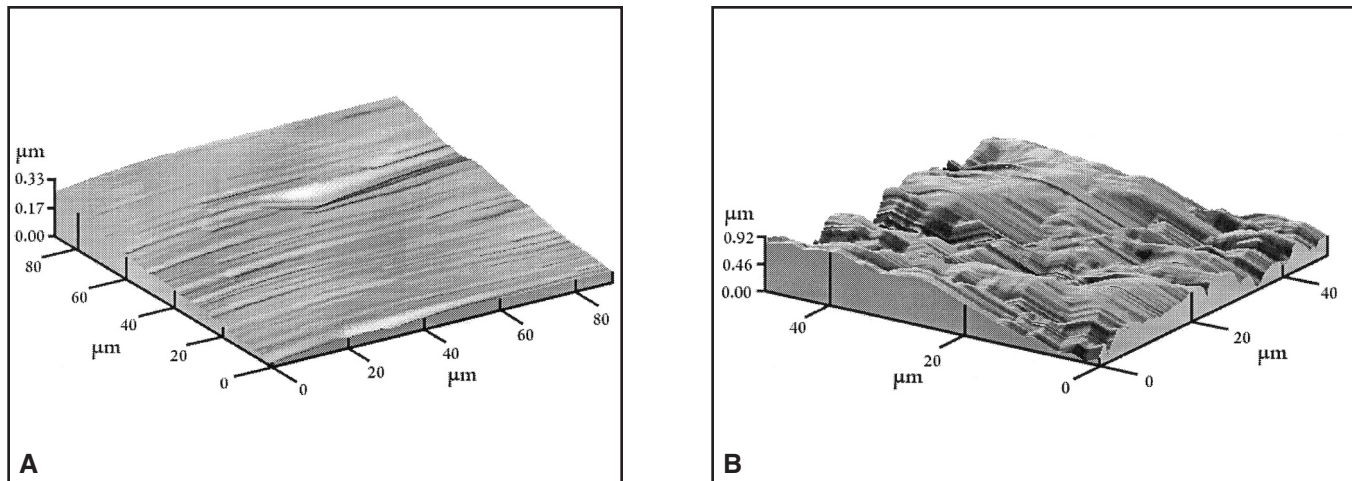


Fig. 3 — AFM images showing regions on the surfaces of (A) polished  $Al_2O_3$  and (B) unpolished  $Al_2O_3$ . The average roughnesses of the polished and unpolished surfaces are, respectively, 28 and 154 nm.

hold at 800°C under an applied load of 0.05 MPa for three grades of roughness. The average roughness,  $R_a$ , was calculated as

$$R_a = \left( \frac{1}{L} \right) \int_0^L f(x) dx \quad (7)$$

where  $L$  is the length of the measured distance and  $f(x)$  is the distance to the surface measured from the centerline. Smoother joining surfaces were found to yield stronger joints in three-point bending with less scatter in the data. The average strength and the Weibull modulus decreased with increasing roughness, while the scatter in the data, as characterized by the standard deviation, increased with increasing roughness.

Suganuma and coworkers (Ref. 42) also explored the effects of surface roughness on the properties of alumina-niobium joints prepared by diffusion brazing. Polycrystalline alumina blocks were bonded to an intervening 1-mm-thick niobium disk using a pressure of 20 MPa for 1 h at 1500°C. The roughness of the polycrystalline alumina and niobium surfaces were varied, with  $R_a$  values of 0.97, 1.62, and 3.1  $\mu\text{m}$ , and 0.41, 2.22, and 3.49  $\mu\text{m}$ , characterizing the alumina and niobium surfaces, respectively. The results of room-temperature four-point bend tests and fractographic analyses were correlated with changes in surface roughness. Increasing alumina roughness resulted in a modest ( $\leq 10\%$ ) decrease in average strength, increased scatter in strength, and a decrease in the area fraction of alumina-niobium contact (98%  $\rightarrow$   $\approx 80\%$ ). In contrast, increasing niobium roughness resulted in a modest ( $\leq 10\%$ ) increase in average strength, and an increase in the area fraction of alumina-niobium contact ( $\approx 80\% \rightarrow \geq 99\%$ ).

## Experimental Procedures

### Joint Processing and Mechanical Testing

The materials and the majority of the experimental procedures used in this work are identical to those of prior studies (Refs. 7, 9, 11, 12). Joints were fabricated using a 99.5% pure,  $\geq 98\%$  dense alumina (AD995, Coors Technical Ceramic Co., Oak Ridge, Tenn.) in the form of 19.5  $\times$  19.5  $\times$  22.5 mm blocks. The joining surfaces of the alumina blocks were ground flat using a diamond wheel (400 grit) on a surface grinder (K. O. Lee Co., Aberdeen, S.Dak.). Joints processed with unpolished alumina substrates were then cleaned while those processed with polished alumina substrates were polished with progressively finer diamond suspensions (South Bay Technologies, San Clemente, Calif.) before cleaning. After polishing with a 1- $\mu\text{m}$  diamond suspension, a final chemical-mechanical polish was performed using colloidal silica (Struers, Westlake, Ohio).

A flattened and cleaned, 99.99% pure, 127- $\mu\text{m}$ -thick niobium foil (Goodfellow Corp., Malvern, Pa.) and a commercial-grade copper (Consolidated Companies Wire and Associated, Chicago, Ill.) served as the interlayer materials. For joints produced via liquid-film-assisted joining, copper films 1.4, 3.0, or 5.5  $\mu\text{m}$  thick were deposited directly onto the polished or unpolished alumina joining surfaces by evaporation of the copper wire source in a high-vacuum chamber. Film thickness was determined using profilometry (Tencor Instruments, Inc., San Jose, Calif.) and weight-gain measurements (Ref. 7).

Joints were processed under high vacuum (pressure maintained below  $7.6 \times 10^{-5}$  torr, equivalent to  $10^{-7}$  atm) in a graphite element vacuum hot press. The brazing process coupled a constant applied load of  $\approx 2.2$  MPa with heating at 4°C/min, soaking at the brazing temperature of 1400°C for 6 h, and cooling at 2°C/min. After brazing, the assemblies were machined into beams  $\approx 3$  mm  $\times$   $\approx 3$  mm in cross section and  $\approx 4$  cm in length,

Table 1 — Surface Roughness\*

| Material            | $R_a$ ( $\mu\text{m}$ ) | $\lambda_a$ ( $\mu\text{m}$ ) | $r$                      | $\alpha_a$ (deg)   |
|---------------------|-------------------------|-------------------------------|--------------------------|--------------------|
| Unpolished alumina  | 0.154 (AFM)             | 8.9 (AFM)                     | 1.014 (AFM)              | 8.7 (AFM)          |
|                     | 0.299, 2.72 (Prof.)     | 30 (Prof.)                    | 1.005, 1.411 (Prof.)     | 4.9, 45.3 (Prof.)  |
| Polished alumina    | 0.027 (AFM)             | 32.5 (AFM)                    | 1.00003 (AFM)            | 0.42 (AFM)         |
|                     | 0.051, 0.057 (Prof.)    | 30 (Prof.)                    | 1.00014, 1.00018 (Prof.) | 0.85, 0.95 (Prof.) |
| As-received niobium | 0.107                   | 11.3                          | 1.0045                   | 4.9                |
| Flattened niobium   | 0.097 (AFM)             | 6.8 (AFM)                     | 1.01 (AFM)               | 7.3 (AFM)          |
|                     | 0.213 (Prof.)           | 20 (Prof.)                    | 1.006 (Prof.)            | 5.3 (Prof.)        |

\*  $R_a$  is the average deviation in surface height,  $\lambda_a$  is the average distance between peaks of surface features,  $r$  is the roughness parameter, and  $\alpha_a$  is the average slope of surface features. Calculations of  $r$  and  $\alpha_a$  use the methods described by Hitchcock et al. (Ref. 43). All values of  $r$  and  $\alpha_a$  were calculated using average values of 50 and 9, respectively, for the arithmetic factors  $K_1$  and  $K_2$ . Where two values are provided, the first is parallel to the scan direction, and the second is perpendicular to the scan direction.

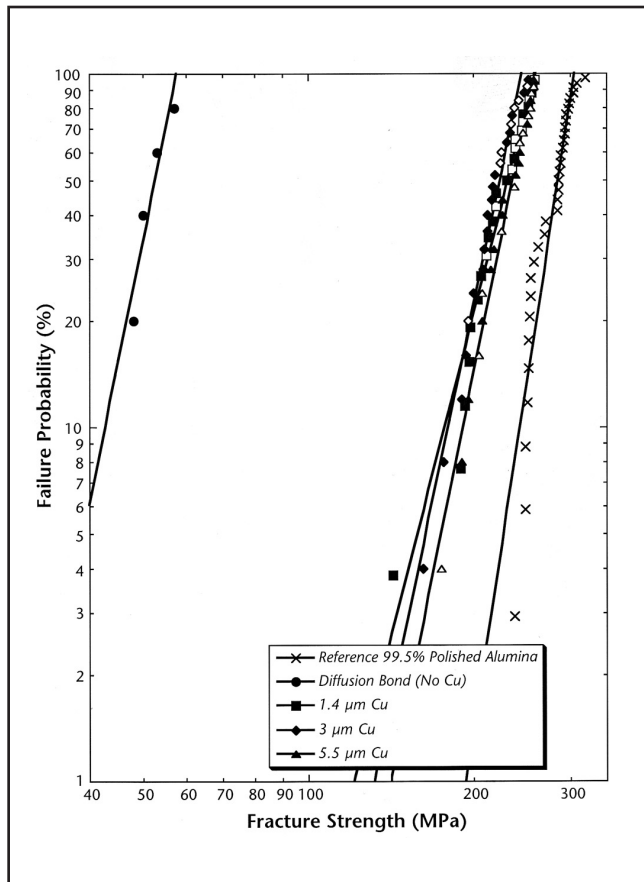


Fig. 4 — Failure probability vs. fracture strength for joints processed with unpolished  $Al_2O_3$  substrates. Filled symbols indicate failure along the  $Al_2O_3$ -Nb interface; open symbols indicate failure in the ceramic.

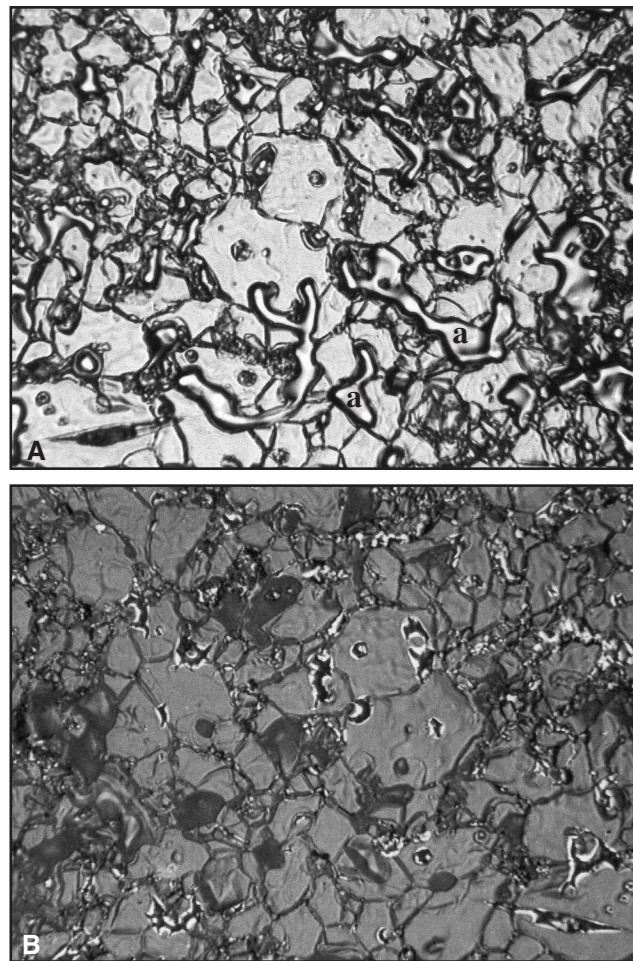


Fig. 5 — Optical micrographs of a polished sample joined with a 5.5- $\mu m$  Cu film, showing matching regions of (A) metal and (B) ceramic sides of the fracture surface. The regions marked “a” indicate unbonded area. The sample failed at 278 MPa.

with the metal interlayer at the center of the beam. The tensile surfaces of the beams were polished to a 1- $\mu m$  finish and the edges of the beams were beveled to remove machining flaws that could initiate failure. This allowed for a more meaningful measurement of the fracture strength of the joined assembly, and the observed fracture path provided insight on the relative strengths of the ceramic-metal interface and the bulk ceramic.

Beams were tested at room temperature using four-point bending. The inner span of the test jig was 9 mm; the outer span was 25 mm. Testing was performed with a displacement rate of 0.05 mm/min. Strengths were calculated from the load at failure using standard relationships derived for monolithic elastic materials.

### Surface and Interface Characterization

The surface roughness of the as-ground and polished alumina blocks, as well as the roughness of the niobium foil before and after flattening, were deter-

mined by atomic force microscopy (AFM) to allow comparison between the surface roughness of the substrates and interlayer and the copper film thickness. The AFM scans typically covered a  $50 \times 50 \mu m$  area, and provided accurate measurements of the local fine-scale roughness. To assess longer wavelength (and larger amplitude) variations in the surface topography, profilometer scans spanning a length of  $\approx 1$  cm were also conducted on polished and as-ground alumina and flattened niobium foils. For the ground alumina, scans were conducted both parallel and perpendicular to the grinding direction. The results are summarized in Table 1. The roughness definitions of Hitchcock et al. (Ref. 43) (see Appendix) were used as the basis for the calculations of the cited roughness values.

For selected samples in which fracture occurred at or near the alumina-interlayer interface, fracture surfaces near the tensile edge were examined using optical microscopy. Fracture surfaces were mounted adjacent to one another so that equivalent

fractographic locations of the metal and ceramic were in mirror symmetry positions. The microstructure at matching locations, the pore structure, and the fracture path could thus be identified.

During bonding, in regions where the ceramic and metal make contact, the ceramic and metal grain boundaries are etched, and the surfaces mutually conform. Thus, when failure occurs along the ceramic-metal interface, an imprint of the ceramic microstructure appears on the metal surface in regions where contact was achieved. The area fractions of contact and interfacial failure (for fracture path statistics) were determined by a point-counting method employing a reference grid superimposed onto a micrograph of the metal fracture surface. The grid was rotated with respect to each micrograph, to yield several distinct grid orientations. Approximately 800 intersection points were evaluated per micrograph. Area fractions were calculated by averaging results for each micrograph, and are reported in Tables 3 and 4.

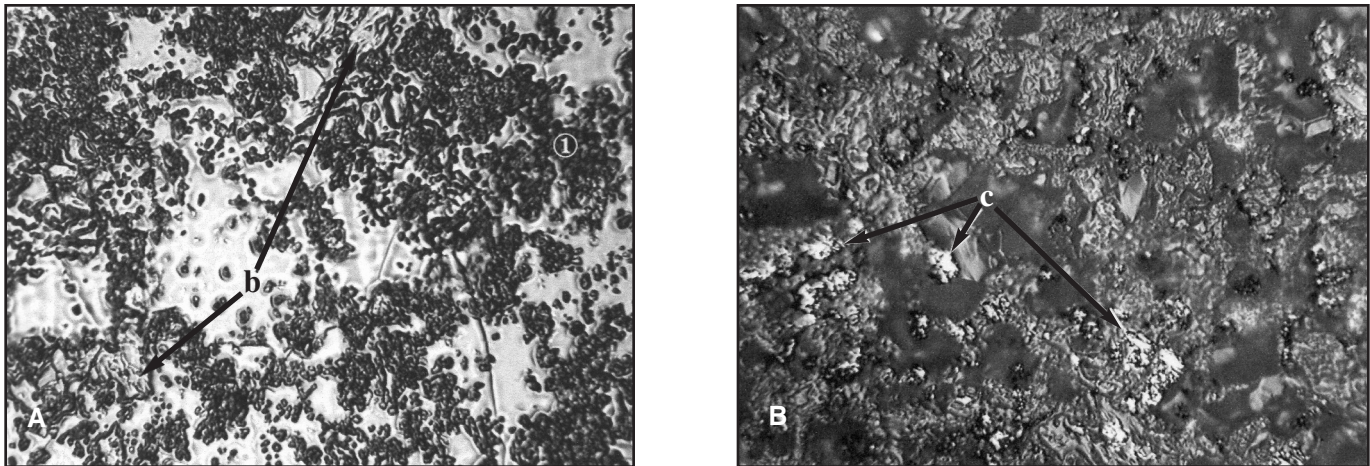


Fig. 6 — Optical micrographs of the fracture surface from an unpolished diffusion bond that failed at 48 MPa, showing matching regions of (A) metal and (B) ceramic sides. The region labeled 1 is deformed metal. The regions marked “b” indicate bonded regions; regions marked “c” indicate the presence of silicides.

## Results and Discussion

### Effects of Copper Thickness and Substrate Roughness on Room-Temperature Mechanical Properties

#### Polished Alumina Substrates

Figure 1 is a plot of failure probability vs. beam fracture strength for bonded assemblies processed with varying copper thicknesses. The alumina “reference” was unbonded and unannealed before testing, and Fig. 1 clearly shows the beneficial effects of thin liquid copper films on the strength characteristics of joined assemblies.

As indicated in Table 1, the three film thicknesses exceed  $R_a$  and are also comparable to or greater than the maximum asperity height ( $0.32 \mu\text{m}$ ) and maximum cavity depth ( $1.38 \mu\text{m}$ ) in profilometry scans of polished alumina. While “flattening” of the niobium foil appears to have little effect on the average roughness, the surface of the flattened niobium contains large divots and depressions. Flattening also increased the roughness parameter,  $r$ , and the average slope of surface features,  $\alpha_a$ , on the niobium foil (see Appendix and Table 1). Figure 2 shows regions on the as-received and flattened niobium foil. During LFAJ, some niobium dissolution occurs. As a result, although large divots and depressions are likely to persist at the bonding temperature, the finer details of the surface topography change. Whether these changes are beneficial or detrimental is unknown. Smoothing and surface faceting are possible depending upon the surface orientation and stability. It is reasonable to expect that in samples prepared using polished alumina and copper films, sufficient liquid should be available to fill most interfacial gaps at the bonding temperature.

Solid-state diffusion brazing at  $1400^\circ\text{C}$  and a pressure of 2.2 MPa led to low average strength, which, in the combined data set taken from two bonded assemblies, was  $130 \pm 20 \text{ MPa}$ ; the Weibull modulus was 5.7. The data do show a kink (dashed lines in Fig. 1) indicating that two failure modes might be operative; however, fractographic analysis showed that all samples failed along the alumina-niobium interface, with considerable tearing of the niobium. Thus, there is no mechanistic basis for such treatment of the data. Interfacial failures at low applied stress were due to large unbonded regions and a high area fraction of interfacial porosity, a consequence of the low applied load and the low rate of solid-state diffusion.

The application of a  $1.4\text{-}\mu\text{m}$  copper film to the bonding surfaces of the alumina substrates increased the average fracture strength to  $197 \pm 37 \text{ MPa}$ . The weakest beam failed at 136 MPa, comparable to the strength of the strongest diffusion-brazed sample (155 MPa). The Weibull modulus was 5.6, essentially the same as that for diffusion brazing. All samples continued to fail along the alumina-niobium interface, but with more limited tearing of the niobium. Here, LFAJ allowed for the filling of interfacial voids by liquid copper and provided a high-diffusivity path for the transport of niobium. Copper dissolves  $\approx 3 \text{ at.-%}$  niobium at  $1400^\circ\text{C}$  (Ref. 31), and the diffusion coefficient for niobium in liquid copper is orders of magnitude higher than the self-diffusion coefficient for niobium. Consequently, the rate of niobium redistribution at the interface during LFAJ can be expected to be much greater than that in conventional solid-state diffusion brazing.

Increasing the copper film thickness to  $3 \mu\text{m}$  yielded a further improvement in the strength to  $241 \pm 18 \text{ MPa}$ , a decrease in standard deviation by slightly more than a

factor of two (from 37 to 18 MPa), and in 71% of samples tested, there is evidence of crack initiation and propagation completely within the ceramic. As Fig. 1 shows, interfacial failures do not necessarily occur at lower stresses. The Weibull modulus increased to 14.9. This is comparable to that of the unbonded reference alumina (13.8).

Prior work had suggested that a further increase in the copper film thickness would degrade the strength characteristics (Ref. 11) due to a larger area fraction of copper at the interface, though no studies had previously been pursued. When the copper film thickness was increased to  $\approx 5.5 \mu\text{m}$ , the average strength increased slightly, from 241 to 246 MPa. However, the standard deviation increased by roughly a factor of two, from 18 to 37 MPa. Only about 57% of the samples failed in the ceramic, but the majority of interfacial failures occurred at lower applied stresses. Samples with the highest ceramic and interfacial fracture strengths failed at stresses of, respectively, 289 and 278 MPa; the lowest ceramic and interfacial failures occurred at stresses of, respectively, 206 and 136 MPa. This spread in the data is far greater than that of samples processed with  $3.0\text{-}\mu\text{m}$  films, as evidenced by the Weibull parameter of 6.0, approximately the value of diffusion-brazed and  $1.4\text{-}\mu\text{m}$ -film assemblies. There is also a large discrepancy between the average fracture strengths and standard deviations for ceramic ( $265 \pm 20 \text{ MPa}$ ) and interfacial ( $223 \pm 41 \text{ MPa}$ ) failures. This degradation in strength is attributed to large regions of copper at the interface. The work of adhesion of an alumina-copper interface is less than that of an alumina-niobium interface (Refs. 35–39). Thicker films are more difficult to break up, and large plate-like copper regions persist at the interface

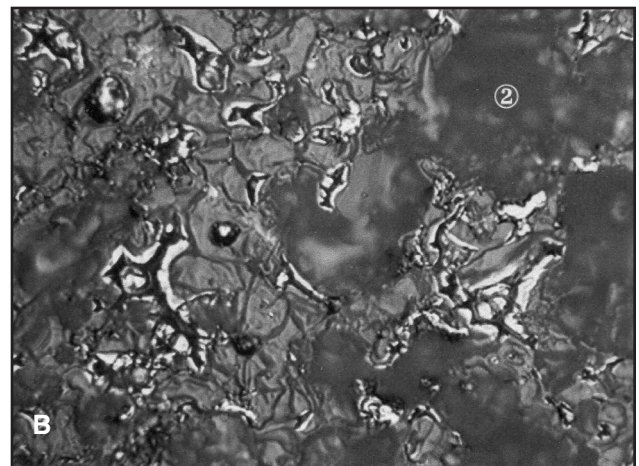
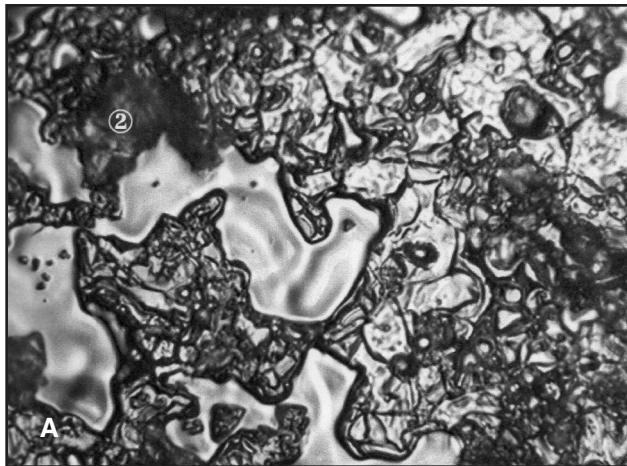


Fig. 7—Optical micrographs from an unpolished sample joined with a 5.5- $\mu\text{m}$  Cu film, showing matching regions of (A) metal and (B) ceramic sides. The region labeled 2 is a ceramic grain that has pulled out and adhered to the metal surface. The sample failed at 246 MPa.

after bonding, yielding higher area fractions of alumina-copper interface.

#### Unpolished Alumina Substrates

Atomic force microscopy (AFM) (Table 1) suggests that it might not be necessary to polish the alumina, since the average roughness of unpolished as-ground surfaces over  $50 \times 50 \mu\text{m}$  areas ( $0.154 \mu\text{m}$ ) remains much less than the minimum liquid film thickness. Similar conclusions are supported by profilometry data over  $50\text{-}\mu\text{m}$  length scales. However, comparisons of profilometry scans over larger distances, up to 1 cm, show significant differences between the polished and as-ground alumina. The  $R_a$  value increased from  $\approx 0.050\text{--}0.060 \mu\text{m}$  for polished alumina to  $0.299\text{--}2.72 \mu\text{m}$  in the as-ground alumina, depending upon the scan direction. Maximum asperity heights increased from  $\approx 0.18\text{--}0.32 \mu\text{m}$  in polished alumina to  $1.7\text{--}14.1 \mu\text{m}$  in as-ground alumina depending upon the scan direction. Maximum surface cavity depths increased from  $1.38 \mu\text{m}$  in polished substrates to  $\approx 11 \mu\text{m}$  in unpolished substrates. In contrast to

polished alumina, the maximum asperity height and cavity depth far exceed even the maximum film thickness. Consequently, unpolished alumina substrates would be more likely to have more severe flaws and larger unbonded regions at the alumina-interlayer interface, and the characteristics of the most severe defects would be relatively insensitive to the film thickness.

Figure 3 provides a comparison of AFM images, and differences are apparent even over limited spatial scales. The flaws on polished alumina surfaces are residual scratches and gouges from grinding, while the flaws on unpolished alumina are more severe. Although the deposited copper film is generally thick enough to fill and cover scratches of this severity at a local scale, point-by-point assessment of 50,000-point profilometry scans of 1 cm total length indicate that  $>3\%$  of the scanned length on the as-ground surface has multiple independent asperities  $>10 \mu\text{m}$  in height. When the ceramic-metal contact initiates at such extreme asperities, large and relatively wide interfacial gaps are anticipated.

Solid-state diffusion brazing was attempted with unpolished alumina substrates, but only 4 of 25 beams survived machining into test samples, and all 4 of these surviving beams failed interfacially at low stresses (48–57 MPa). Large unbonded areas, high porosity, and deviations from planarity that introduce local stress concentrations at the interface, all contribute to crack initiation and failure.

Figure 4 is a plot of failure probability vs. beam fracture strength for bonded assemblies processed with varying copper thicknesses. The average strength of joints processed with copper films of 1.4, 3, and  $5.5 \mu\text{m}$  are, respectively,  $224 \pm 27 \text{ MPa}$ ,  $218 \pm 23 \text{ MPa}$ , and  $230 \pm 24 \text{ MPa}$ , demonstrating that the thickness of the copper film has little effect on the strength characteristics of assemblies processed with unpolished alumina substrates. The average roughness of unpolished alumina substrates is  $0.299$  and  $2.7 \mu\text{m}$  in orthogonal directions. Filling a sawtooth surface profile with average surface asperity height of  $2.7 \mu\text{m}$  and average surface cavity depth of  $2.7 \mu\text{m}$  would require at least  $2.7 \mu\text{m}$  of copper. However, if during bonding the peaks on the alumina surface became embedded in the niobium and liquid copper were displaced to adjoining regions, thinner films could be sufficient to fill interfacial gaps. Unfortunately, the most severe height deviations in the as-ground alumina surface create significantly larger interfacial gaps. Displacement of liquid copper into these most severe interfacial gaps would reduce their size, but could not fill them completely. Consequently, the statistical distribution of such flaws at the interface may explain the observed strength characteristics.

Fracture characteristics appear to improve slightly with increasing film thickness (Table 2). The Weibull modulus in-

Table 2—Strength Characteristics

| Substrate Finish          | Film Thickness ( $\mu\text{m}$ ) | Average Strength (MPa) | Weibull Modulus | Ceramic Failures (%) |
|---------------------------|----------------------------------|------------------------|-----------------|----------------------|
| Polished                  | 0                                | 103 ( $\pm 20$ )       | 5.7             | 0                    |
| Unpolished <sup>(a)</sup> | 0                                | 52 ( $\pm 4$ )         | —               | 0                    |
| Polished                  | 1.4                              | 197 ( $\pm 37$ )       | 5.6             | 0                    |
| Unpolished                | 1.4                              | 224 ( $\pm 27$ )       | 8.0             | 40                   |
| Polished                  | 3.0                              | 241 ( $\pm 18$ )       | 14.9            | 71                   |
| Unpolished                | 3.0                              | 218 ( $\pm 23$ )       | 10.0            | 29                   |
| Polished                  | 5.5                              | 246 ( $\pm 37$ )       | 6.0             | 57                   |
| Unpolished                | 5.5                              | 230 ( $\pm 24$ )       | 10.2            | 46                   |

(a) Only four out of a possible 25 beams survived the machining process.

creases from 8.0 for the 1.4- $\mu\text{m}$  film to 10.0 for the 3.0- $\mu\text{m}$  film to 10.2 for the 5.5- $\mu\text{m}$  film. In bonds prepared with polished substrates, the maximum Weibull modulus (14.9) coincided with the highest percentage of ceramic failures (71% for 3.0- $\mu\text{m}$  films). In the present case, the percentages of failures that occur in the ceramic for 1.4-, 3.0-, and 5.5- $\mu\text{m}$  films are, respectively, 40%, 29%, and 46%. Thus, the Weibull modulus does not parallel the percentage of ceramic failures, but seems to increase with film thickness.

Under optimum conditions, joints processed with polished substrates exhibit slightly better strength characteristics than those processed with unpolished substrates, and have higher values of the Weibull modulus. However, for many applications unpolished substrates may be adequate and even desirable, especially since elimination of the polishing process would save considerable time and reduce cost. Further research and more data would be helpful to augment the statistics presented here in support of such decisions.

### Fractography

Fractography was performed on diffusion-brazed and LFAJ samples in both polished and unpolished conditions. For all images, the tensile surface lies near the adjacent edges of the micrographs showing the metal (A) and ceramic (B) sides of the fracture surface.

By comparing the extent to which the ceramic microstructure was imprinted on the metal surface (Refs. 7, 9, 11, 12, 14, 44, and 45), regions in which contact was not achieved during bonding were identified. In diffusion-brazed samples, approximately one-half of the interface was obscured. The ceramic side of the interface was obscured by adherent islands of metal or silicide (Refs. 13, 46, 47); the metal side of the interface was obscured by deformed metal (labeled ① in Fig. 6A) or adherent alumina grains (labeled ② in Fig. 7). The observable regions of contact are therefore only within the fraction of the total fracture surface associated with interfacial failure. An upper limit on the area fraction of contact is obtained by assuming that regions in which the crack deviates from the interface are associated with complete alumina-niobium contact. However, if the interfacial porosity is uniformly distributed, the average area fraction of contact is given by the area fraction of contact within regions of interfacial failure. This latter interpretation seems to better rationalize the significant strength differences between diffusion-brazed and LFAJ samples (Ref. 12). Both values are provided in Tables 3 and 4 for polished and unpolished samples, respectively. For unpolished

**Table 3 — Fracture Path and Contact Area Statistics for Polished Assemblies**

|  | Fracture Path Statistics          |   | Area Fraction Bonded  |  |
|--|-----------------------------------|---|---|--|
|  | Area Fraction Interfacial Failure | Area Fraction Interlayer or Ceramic Failure | $1 - \frac{\text{Area}_{\text{unbonded}}}{\text{Area}_{\text{fracture surface}}}$ | $1 - \frac{\text{Area}_{\text{unbonded}}}{\text{Area}_{\text{interfacial failure}}}$ |
| <b>Diffusion bond</b>                  |                                   |   |   |  |
| 79 MPa                                 | 0.495                             | 0.505                                       | 0.812   | 0.621  |
| 102 MPa                                | 0.473                             | 0.527                                       | 0.809   | 0.572  |
| 119 MPa                                | 0.54                              | 0.46  | 0.813   | 0.595  |
| <b>1.4 <math>\mu\text{m}</math> Cu</b> |                                   |   |   |  |
| 136 MPa                                | 0.695                             | 0.305                                       | 0.84  | 0.77   |
| 197 MPa                                | 0.665                             | 0.335                                       | 0.877   | 0.808  |
| 260 MPa                                | 0.68                              | 0.32  | 0.938   | 0.908  |
| <b>3.0 <math>\mu\text{m}</math> Cu</b> |                                   |   |   |  |
| 206 MPa                                | 0.965                             | 0.035                                       | 0.843   | 0.837  |
| 243 MPa                                | 0.897                             | 0.103                                       | 0.788   | 0.764  |
| 263 MPa                                | 0.95                              | 0.05  | 0.97  | 0.968  |
| <b>5.5 <math>\mu\text{m}</math> Cu</b> |                                   |   |   |  |
| 192 MPa                                | 0.721                             | 0.279                                       | 0.765   | 0.674  |
| 213 MPa                                | 0.744                             | 0.256                                       | 0.903   | 0.87   |
| 261 MPa                                | 0.686                             | 0.314                                       | 0.929   | 0.897  |

**Table 4 — Fracture Path and Contact Area Statistics for Unpolished Assemblies**

|  | Fracture Path Statistics          |   | Area Fraction Bonded  |  |
|--|-----------------------------------|---|---|--|
|  | Area Fraction Interfacial Failure | Area Fraction Interlayer or Ceramic Failure | $1 - \frac{\text{Area}_{\text{unbonded}}}{\text{Area}_{\text{fracture surface}}}$ | $1 - \frac{\text{Area}_{\text{unbonded}}}{\text{Area}_{\text{interfacial failure}}}$ |
| <b>Diffusion bond</b>                  |                                   |   |   |  |
| 48 MPa                                 | 0.451                             | 0.549                                       | 0.679   | 0.288  |
| 57 MPa                                 | 0.489                             | 0.511                                       | 0.679   | 0.344  |
| <b>1.4 <math>\mu\text{m}</math> Cu</b> |                                   |   |   |  |
| 213 MPa                                | —                                 | —   | 0.687   | —  |
| 246 MPa                                | —                                 | —   | 0.686   | —  |
| <b>3.0 <math>\mu\text{m}</math> Cu</b> |                                   |   |   |  |
| 216 MPa                                | —                                 | —   | 0.647   | —  |
| 242 MPa                                | —                                 | —   | 0.729   | —  |
| <b>5.5 <math>\mu\text{m}</math> Cu</b> |                                   |   |   |  |
| 218 MPa                                | —                                 | —   | 0.699   | —  |
| 246 MPa                                | —                                 | —   | 0.809   | —  |

samples processed with copper films, there does not appear to be any tearing of the niobium foil, and hence there is no obscured interface. Although more ceramic pullout occurs than in polished samples, the failure is predominantly interfacial, and thus, only a single value is reported.

### Polished Alumina Substrates

Increasing the copper thickness affected both the strength and the fracture path. Comparing the fracture surfaces of samples processed with 0-, 1.4-, 3.0-, and 5.5- $\mu\text{m}$  copper films, the average area fraction of interfacial failure was  $\approx 48(\pm 5)\%$ ,  $\approx 67(\pm 6)\%$  (Ref. 12),  $\approx 94(\pm 5)\%$ , and  $\approx 71(\pm 10)\%$ , respectively. However, it should be noted that the per-

centage of samples that fail along the interface varies with copper film thickness (Table 2). In samples with no copper and 1.4- $\mu\text{m}$  films, significant tearing of the niobium interlayer occurred, along with regions where there was no contact between the alumina and niobium interlayer. Niobium tearing and unbonded regions are much more limited in samples processed with 3.0- and 5.5- $\mu\text{m}$  films. In these samples, better contact was achieved, and ceramic grains pull out and adhere to the niobium fracture surface. However, the 5.5- $\mu\text{m}$  copper films resulted in an increase in the number of interfacial failures and unbonded regions as compared to 3.0- $\mu\text{m}$  samples. Figure 5 shows the metal and ceramic fracture surfaces of a sample that failed at 278 MPa. The copper particles at

the interface tear during fracture, and there is a slight increase in niobium tearing relative to samples processed with a 3.0- $\mu\text{m}$  film (see Table 3, Area Fraction Interlayer or Ceramic Failure). There are still large unbonded regions between the alumina and niobium (indicated as "a" in Fig. 5A), and the area fraction of these regions decreased as the fracture strength increased. The increase in interfacial failures correlates with a slight increase in the amount of copper in the braze, increasing the area fraction of alumina-copper interface.

#### Unpolished Alumina Substrates

Fractography of a diffusion-brazed sample that failed at 48 MPa is shown in Fig. 6. From inspection of the metal side (Fig. 6A), it is evident that the majority of the interface remained unbonded. Small regions of bonding between the alumina and niobium are marked "b" in Fig. 6A. Niobium grain boundaries are seen in the large unbonded regions. Energy-dispersive spectroscopy in both SEM (Ref. 13) and TEM (Refs. 46, 47), and electron diffraction analysis (Refs. 46, 47) indicate that silicides form in regions of alumina with small grains. These silicide particles appear as bright regions on the ceramic side of the interface, and are labeled "c" in Fig. 6B. The low strength of these samples is a result of poor contact between the alumina and niobium due to the roughness of the alumina substrates.

Figure 7 shows metal and ceramic sides of a sample processed with a 5.5- $\mu\text{m}$  copper film that failed at 246 MPa. The fracture surfaces for the three film thicknesses do not appear to show any major differences, which is to be expected based on the similar strength characteristics. The bonded area fraction is approximately the same for all samples (Table 4). Comparing mating fracture surfaces, the unbonded regions on the metal side correspond with regions on the alumina side that are darker in contrast. Such unbonded regions are attributed to large localized depressions on the alumina surface, as shown in Fig. 7. The amount of copper on the fracture surfaces appears to increase slightly with increasing film thickness, but does not appear to have had any significant effect on the strength characteristics. There is also more ceramic pullout in these samples relative to polished samples, possibly indicative of grinding-induced near-surface damage. These regions that pulled out and adhered to the metal surfaces are elevated regions on the alumina joining surfaces. Better contact relative to surface depressions can be made with the niobium during the bonding cycle, since these elevated regions will penetrate and deform

the metal layer due to the applied pressure and temperature. The majority of samples that failed interfacially also exhibited small regions of ceramic along the tensile edge that adhered to the niobium foil, indicating a more tortuous crack path.

#### Polished vs. Unpolished Substrates

For samples that fail primarily along the alumina-interlayer interface, the differences between the fracture surfaces of polished and unpolished substrates are evident upon inspection. The individual unbonded regions are significantly larger in the unpolished samples than in the polished samples (see Figs. 5 and 7, both processed with 5.5- $\mu\text{m}$  copper films), and the bonded area fraction is lower in unpolished samples. The copper distribution is also different. Again comparing samples with 5.5- $\mu\text{m}$  copper films, the average area fraction of copper coverage in unpolished samples ( $\approx 13\%$ ) is roughly twice that in polished samples ( $\approx 7\%$ ), and the average projected area of residual copper patches is three to four times larger in unpolished samples,  $\approx 11\text{--}17\ \mu\text{m}^2$  vs.  $\approx 4\ \mu\text{m}^2$ . As a result, copper is more uniformly dispersed and isolated patches are smaller in the polished specimens.

These general microstructural differences exist regardless of the copper film thickness. At constant copper film thickness, the only variable is the alumina surface roughness. Therefore, it is useful to assess and rationalize how a change in roughness could cause or contribute to the observed microstructural trends.

Models of solid-state metal-metal diffusion brazing (Refs. 48, 49) depict the earliest stages of bonding as asperity contact, and for small contact area, the applied stress is large. In the present ceramic-metal case, asperities on the alumina surface will likely be pushed into the softer niobium, increasing the contact area until the stresses decrease to the niobium yield stress. Increasing the applied load promotes more extensive contact formation during this initial stage, and reduces the size of interfacial defects. Interfacial gaps flank large asperities and deep depressions in the alumina. Copper, once molten, can withdraw from or redistribute within these cavities leaving voids at the alumina-niobium interface, which, if they persist, provide potential sites for crack/failure initiation. As the contact area increases, regions of the interface become isolated by continuous perimeters of ceramic-metal contact. Pockets completely filled with liquid increase the effective area supporting the applied load. Since access to additional copper by liquid flow is precluded, if these isolated regions are not completely filled with copper at

the bonding temperature, void closure and the development of full contact will require either additional deformation/creep of the foil or longer-range diffusion. In view of the significant differences in asperity heights, significant differences between interfacial microstructures and fracture characteristics in polished and unpolished samples can be expected. Even when the cavities are filled at the bonding temperature, voids within the copper are expected at room temperature. The differential thermal expansion of copper relative to niobium and alumina, and the volume change due to copper solidification, are expected to generate  $\approx 12\ \text{vol-}\%$  porosity within the copper-rich phase.

Bonding experiments using highly polished (transparent) single-crystal sapphire substrates have allowed nondestructive studies of the morphological evolution of the copper film and the growth of sapphire-niobium contact during postbonding annealing (Ref. 50). The results confirm that sapphire-niobium contact initiates at asperities on the adjoining surfaces. Some of these asperities are initially present on the bonding surfaces, while others form and grow during bonding and subsequent annealing, such as those due to liquid copper etching niobium grain boundaries and forming grain boundary grooves. Pairs of protruding ridges that flank each grain boundary groove develop on the niobium surface and grow to locally bridge the liquid copper film. Subsequent capillary instabilities at the edges of copper patches lead to film breakup and the isolation of small copper particles along the sapphire-niobium interface.

In the present work, the initial points of contact and the progressive growth of alumina-niobium contact are highly influenced by the alumina surface roughness. Since the roughness of the polished samples approaches that of the sapphire substrates, it is reasonable to assume that the early stages of contact formation will again be ridges due to preexistent asperities and grain boundary grooves, and the spacing and location of these points of contact will be a function of the surface topography and the niobium grain size. Grooving of the alumina grain boundaries and faceting of alumina grains may also contribute to the breakup and evolution of the copper film. Recent work by Saiz et al. (Ref. 51) has demonstrated enhanced rates of alumina grain boundary grooving at liquid-metal-alumina interfaces.

Prior work by Suganuma et al. (Ref. 42) and findings in the present study (see Tables 3 and 4) provide evidence of a decrease in the area fraction of contact achieved during solid-state bonding as the roughness of the alumina increases. A substantially larger height difference be-

tween initial points of contact and valleys in the alumina surface make it more difficult to achieve complete ceramic-metal contact in both diffusion brazing and LFAJ of unpolished samples. Larger interfacial gaps relative to polished samples may also reduce the impact of grain boundary groove ridging on film breakup.

Optical microscopy of cross sections normal to the alumina-niobium interface prepared from bend beams that failed in the ceramic reveals that the niobium conforms to the alumina topography. Niobium is pushed into depressions (e.g., pores) in the alumina surface and deforms to accommodate elevations on the alumina surface. In unpolished samples, local elevations in the alumina surface of up to several microns are evident along the interfaces. These may define the initial points and areas of alumina-niobium contact and define gaps between the alumina and niobium surfaces during the initial stages of bonding that are larger than would be inferred from either the AFM or averaged profilometry data.

In unpolished samples that fail along the interface, fracture surfaces suggest the gaps are too large for complete removal. Isolated, rough mottled regions on the metal side of the fracture surface are believed to reflect the imprint of rough elevated regions on the alumina surface as they are forced into the niobium. The flow and removal of copper liquid from these regions of contact and the low joining temperature inhibit decay of the resulting interfacial roughness. The resulting roughness at the interface will provide a more tortuous interfacial crack path relative to that of the polished samples.

The difference in the roughness of the alumina can also affect the redistribution of copper along the interface during processing and its ultimate morphology. An important issue is whether gaps larger than the local thickness of the copper film can be filled by liquid flow. If the contact angles of liquid copper on niobium and alumina are denoted  $\theta_1$  and  $\theta_2$ , respectively, and the niobium and alumina surfaces are parallel, then liquid copper flows into voids along the interface provided that  $\theta_1 + \theta_2 < 180$  deg. If instead, local depressions on the opposing niobium and alumina surfaces cause angular deviations of  $\alpha_1$  and  $\alpha_2$ , respectively, from this parallel surface geometry, then flow of liquid into voids will only occur if a more stringent condition,  $(\theta_1 + \alpha_1) + (\theta_2 + \alpha_2) < 180$  deg, is met. Since  $\theta_1$  and  $\theta_2$  can vary as the surface orientations and surface energies of the niobium and alumina grains vary, and  $\alpha_1$  and  $\alpha_2$  will vary with location along the interface, the potential exists for some regions of the interface to have unfavorable wetting conditions. A rougher surface

with locally larger values of  $\alpha_1$  and  $\alpha_2$  would be more likely to contain voids that persist or develop during liquid flow (see Table 1).

For polished surfaces, long-wavelength variation in the alumina-niobium separation distance will cause longer-range liquid redistribution, with liquid drawn into thinner gaps. For rough surfaces, the copper is more likely to be confined by alumina-asperity-niobium contact, precluding longer-range flow of the liquid and resulting in larger residual voids at the interface. In isolated interfacial cavities partially filled with liquid copper, copper coating the depressions in the alumina will tend to flow out of these "deep" regions to the perimeter where it will contact the niobium. These copper pools are seen along the perimeters of valleys on the alumina surface.

The presence of interfacial copper particles can have a beneficial effect on the fracture toughness of bonded assemblies. Kruzic et al. (Ref. 13) have estimated a toughening contribution of 22 J/m<sup>2</sup> or  $\approx 60\%$  of the room-temperature fracture energy (39 J/m<sup>2</sup>) in polished samples processed with a 3.0- $\mu\text{m}$  copper film. The analysis of Kruzic et al. (Ref. 13) furthermore predicts a linear relation between particle size and the increment of interfacial toughness, and thus, provided the shapes of the particles are the same, a higher degree of toughening is expected when more and larger copper particles are present. Due to the interplay between surface roughness and liquid redistribution during LFAJ, for a fixed copper layer thickness, the individual copper islands are larger and most likely thicker in unpolished samples. However, the geometry of the metal phase is also important. Experimental observations have shown that increasing the area fraction of the alumina-copper interface has a detrimental effect when the copper is in the form of a continuous thin film. Fracture studies of tantalum nitride-copper interfaces by Dauskardt et al. (Ref. 52) show a change from a ductile mode to a brittle mode when the copper thickness falls below  $\approx 1$   $\mu\text{m}$ . Consequently, the detailed morphology of the metal phase, and specifically the extent to which the film has evolved into discrete and more equiaxed particles, may play an important role in defining the magnitude of any toughening resulting from metal plasticity and particle tearing.

In the present study, a single variation in the surface finish was explored and processing times were held fixed as the copper film thickness and surface finish were varied. Ideally, adjustments in the surface finish can be used to alter the initial copper particle morphology and distribution, and modifications in the processing time

or postbonding annealing can be used to further tune the morphology. The potential therefore exists to further improve the failure characteristics and maximize the contribution of ductile copper particles to interfacial toughening.

## Conclusions

Alumina-niobium interfaces were fabricated via diffusion brazing and liquid-film-assisted joining (LFAJ) at 1400°C with an applied load of  $\approx 2$  MPa. The initially continuous copper film is designed to redistribute by liquid flow, facilitate the filling of interfacial voids, and provide a high transport rate path for dissolved niobium to accelerate alumina-niobium contact growth. Copper film thicknesses were varied on the surfaces of polished and unpolished alumina substrates. For polished substrates, the average fracture strength increased and the standard deviation decreased as the thickness of the copper film was increased progressively from 0  $\mu\text{m}$  to 1.4  $\mu\text{m}$  to 3.0  $\mu\text{m}$ . As shown in Fig. 1 and Table 2, the average fracture strength then increased slightly but the standard deviation also increased as the copper film thickness increased to 5.5  $\mu\text{m}$ , indicating that a 3.0- $\mu\text{m}$  copper film is the optimum thickness on polished substrates.

For unpolished substrates, the introduction of a copper film also resulted in joints with higher average fracture strength. However, in contrast to polished substrates, varying the thickness of the copper film from 1.4 to 5.5  $\mu\text{m}$  had little effect on the fracture characteristics of unpolished substrates, as shown in Fig. 4. Since the only difference between the two sets of samples is the alumina surface preparation, this suggests that when unpolished alumina is used, some characteristic of the alumina surface emerges as a more dominant factor controlling the strength. The unpolished substrates have a significantly higher  $R_a$  value (Table 1), and grinding may also introduce near-surface flaws that are more severe than in the polished samples. The close coincidence of the strength data for the three film thicknesses (Fig. 4) suggests that in unpolished samples larger unfilled voids along the interface (Fig. 7), or near-interfacial flaws, or both define a nearly constant effective critical flaw size. Polished substrates appear to exhibit slightly better strength characteristics than unpolished substrates (Table 2), but the benefits may not be significant enough to require polishing of the joining surfaces in all cases.

Fractography of specimens that failed interfacially indicates that the fracture path and area fraction of contact between alumina and niobium are affected by cop-

per film thickness in samples produced with polished substrates but not in samples produced with unpolished substrates, as summarized in Tables 3 and 4. For polished substrates, there is progressively less tearing of the niobium interlayer with increasing copper film thickness. There is a transition from mainly interfacial failure to ceramic failure at a thickness of 3.0  $\mu\text{m}$ . The area fraction of contact increases with increasing film thickness to 3.0  $\mu\text{m}$ , then decreases when the film thickness is increased further to 5.5  $\mu\text{m}$ . For unpolished substrates, the fracture path and area fraction of contact are unaffected by the copper film thickness. The interfacial morphologies of samples produced with polished surfaces and unpolished surfaces are significantly different.

#### Acknowledgments

This research was supported by the Director, Office of Science, Office of Basic Energy Sciences, Division of Materials Science and Engineering, of the U.S. Department of Energy under Contract No. DE-AC03-76SF00098. The efforts of Daniel Carvajal in performing the area-fraction measurements are gratefully acknowledged.

#### References

1. Nicholas, M. G., Forgan, R. R. G., and Poole, D. M. 1968. The adhesion of metal/alumina interfaces. *J. Mater. Sci.* 3: 9–14.
2. Florjancic, M., Mader, W., Rühle, M., and Turwitt, M. 1985. HREM and diffraction studies of an  $\text{Al}_2\text{O}_3/\text{Nb}$  interface. *J. Phys. (Paris)* 46(C4): 129–33.
3. Burger, K., Mader, W., and Rühle, M. 1987. Structure, chemistry and diffusion bonding of metal/ceramic interfaces. *Ultramicroscopy* 22(1–4): 1–14.
4. Mader, W., and Rühle, M. 1989. Electron microscopy studies of defects at diffusion-bonded  $\text{Nb}/\text{Al}_2\text{O}_3$  interfaces. *Acta Metall.* 37(3): 853–66.
5. Mayer, J., Flynn, C. P., and Rühle, M. 1990. High-resolution electron microscopy studies of  $\text{Nb}/\text{Al}_2\text{O}_3$  interfaces. *Ultramicroscopy* 33(1): 51–61.
6. O'Dowd, N. P., Stout, M. G., and Shih, C. F. 1992. Fracture toughness of alumina-niobium interfaces: Experiments and analyses. *Philos. Mag. A, Phys. Condens. Matter Defects Mech. Prop. (UK)* 66(6): 1037–64.
7. Shalz, M. L., Dalgleish, B. J., Tomsia, A. P., Cannon, R. M., and Glaeser, A. M. 1994. Ceramic joining III bonding of alumina via  $\text{Cu}/\text{Nb}/\text{Cu}$  interlayers. *J. Mater. Sci.* 29(14): 3678–90.
8. Rühle, M. 1995. Structure and composition of metal/ceramic interfaces. *J. Eur. Ceram. Soc.* 16(3): 353–65.
9. Marks, R. A., Chapman, D. R., Danielson, D. T., and Glaeser, A. M. 2000. Joining of alumina via copper/niobium/copper interlayers. *Acta Mater. (USA)* 48(18–19): 4425–38.

10. Knauss, D., and Mader, W. 1991. Chemical composition and lattice relaxations at diffusion-bonded  $\text{Nb}/\text{Al}_2\text{O}_3$  interfaces. *Ultramicroscopy* 37(1–4): 247–262.
11. Marks, R. A., Sugar, J. D., and Glaeser, A. M. 2001. Ceramic joining IV. Effects of processing conditions on the properties of alumina joined via  $\text{Cu}/\text{Nb}/\text{Cu}$  interlayers. *J. Mater. Sci.* 36(23): 5609–24.
12. Sugar, J. D., McKeown, J. T., Marks, R. A., and Glaeser, A. M. 2002. Liquid-film assisted formation of alumina-niobium interfaces. *J. Am. Ceram. Soc.* 85(10): 2523–30.
13. Kruzic, J. J., Marks, R. A., Yoshiya, M., Glaeser, A. M., Cannon, R. M., and Ritchie, R. O. 2002. Fracture and fatigue behavior at ambient and elevated temperatures of alumina bonded with copper/niobium/copper interlayers. *J. Am. Ceram. Soc.* 85(10): 2531–41.
14. Ellsner, G., Reidel, S., and Pabst, R. 1975. Fractography and fracture paths in ceramic-metal composites. *Prakt. Metallogr.* 12(5): 234–43.
15. Morozumi, S., Kikuchi, M., and Nishino, T. 1981. Bonding mechanism between alumina and niobium. *J. Mater. Sci.* 16(8): 2137–44.
16. Turwitt, M., Ellsner, G., and Petzow, G. 1985. Manufacturing and mechanical properties of interfaces between sapphire and niobium. *J. Phys. (Paris)* 46(C4): 123–27.
17. Rühle, M., Burger, K., and Mader, W. 1986. Structure and chemistry of grain boundaries in ceramics and of metal/ceramic interfaces. *J. Microsc. Spectrosc. Electron* 11(3): 163–77.
18. Rühle, M., Backhaus-Ricoult, M., Burger, K., and Mader, W. 1987. Diffusion bonding of metal/ceramic interfaces — A model study at the  $\text{Nb}/\text{Al}_2\text{O}_3$  interfaces. Ed. J. A. Pask and A. G. Evans. *Proceedings of Ceramic Microstructures '86*. New York, N.Y.: Plenum Press, pp. 295–305.
19. Fischmeister, H. F., Mader, W., Gibbesch, B., and Ellsner, G. 1988. Preparation, properties, and structure of metal/oxide interfaces. *Mater. Res. Soc. Symp. Proc.* Ed. W. A. T. Clark, C. L. Briant, and M. H. Yoo. Materials Research Society, pp. 529–40.
20. Rühle, M., and Evans, A. G. 1989. Structure and chemistry of metal/ceramic interfaces. *Mater. Sci. Eng.* A107: 187–87.
21. Burger, K., and Rühle, M. 1989. Material transport mechanisms during the diffusion bonding of niobium to  $\text{Al}_2\text{O}_3$ . *Ultramicroscopy* 29(1–4): 88–97.
22. Mader, W. 1989. Structure and chemistry of interfaces between oxide precipitates and a metal matrix. *Z. Metallkde.* 80(3): 139–51.
23. Kuwabara, M., Spence, J. C. H., and Rühle, M. 1989. On the atomic structure of the  $\text{Nb}/\text{Al}_2\text{O}_3$  interface and the growth of  $\text{Al}_2\text{O}_3$  particles. *J. Mater. Res. Soc.* 4(4): 972–77.
24. Ohuchi, F. S. 1989. Surface science studies of  $\text{Nb}$ -(0001) $\text{Al}_2\text{O}_3$  interfacial reactions. *J. Mater. Sci. Lett.* 8(12): 1427–9.
25. Mayer, J., Dura, J., Flynn, C. P., and Rühle, M. 1990. Electron microscopy studies of  $\text{Nb}-\text{Al}_2\text{O}_3$  interfaces formed by molecular beam epitaxy. *Surface and Coatings Technol.* 43/44: 199–212.
26. Reimanis, I. E. 1992. Pore removal during diffusion bonding of  $\text{Nb}-\text{Al}_2\text{O}_3$  interfaces. *Acta Metall. Mater., Suppl.* 40: S67–74.
27. Ellsner, G., Korn, D., and Rühle, M. 1994. The influence of interface impurities on

fracture energy of UHV diffusion bonded metal-ceramic bicrystals. *Scr. Metall. Mater.* 31(8): 1037–42.

28. Gupta, V., Wu, J., and Pronin, A. N. 1997. Effect of substrate orientation, roughness, and film deposition mode on the tensile strength and toughness of niobium-sapphire interfaces. *J. Am. Ceram. Soc.* 80(12): 3172–80.
29. Soyez, G., Ellsner, G., Rühle, M., and Raj, R. 1998. Constrained yielding in niobium single crystals bonded to sapphire. *Acta Mater. (USA)* 46(10): 3571–81.
30. Zhang, W., and Smith, J. R. 2000. Stoichiometry and adhesion of  $\text{Nb}/\text{Al}_2\text{O}_3$ . *Phys. Rev. B* 61(24): 883–89.
31. Massalski, T. B. 1990. *Binary Alloy Phase Diagrams*. Metals Park, Ohio: ASM International.
32. Hodkin, E. N., Nicholas, M. G., and Poole, D. M. 1970. The surface energies of solid molybdenum, niobium, tantalum and tungsten. *J. Less-Common Met.* 20(2): 93–103.
33. De Lima, O. F., Krehl, M., and Schulze, K. 1985. Wetting characteristics of copper on niobium. *J. Mater. Sci.* 20(7): 2464–70.
34. Locatelli, M. R., Tomsia, A. P., Nakashima, K., Dalgleish, B. J., and Glaeser, A. M. 1995. New strategies for joining ceramics for high-temperature applications. *Key Eng. Mater.* 111–12: 157–90.
35. Liu, W., Ellsner, G., and Rühle, M. 2001. Effects of thin film Nb interlayer in  $\text{Cu}/\text{sapphire}$  bonds. *Mater. Sci. Eng.* A317: 153–62.
36. Girifalco, L. A., and Good, R. J. 1957. A theory for the estimation of surface and interfacial energies I. Derivation and application to interfacial tension. *J. Phys. Chem.* 61(7): 904–8.
37. Jilavi, M. 1994. Ph.D. dissertation. Stuttgart, Germany: University of Stuttgart.
38. Eustathopoulos, N., Chatain, D., and Coudurier, L. 1991. Wetting and interfacial chemistry in liquid metal-ceramic systems. *Mater. Sci. Eng.* A135: 83–88.
39. Li, J. G. 1992. Wetting and interfacial bonding of metals with ionocovalent oxides. *J. Am. Ceram. Soc.* 75(11): 3118–26.
40. Suganuma, K., Okamoto, T., Koizumi, M., and Shimada, M. 1986. Effects of surface damage on strength of silicon nitride bonded with aluminum. *Advanced Ceram. Mater.* 1(4): 356–60.
41. Suganuma, K., Miyamoto, Y., and Koizumi, M. 1988. Joining of ceramics and metals. *Ann. Rev. Mater. Sci.* 18: 47–73.
42. Suganuma, K., Okamoto, T., and Koizumi, M. 1989. Effect of surface grinding conditions on strength of alumina/niobium joint. *Ceram. Eng. Sci. Proc.* 10(11–12): 1919–33.
43. Hitchcock, S. J., Carroll, N. T., and Nicholas, M. G. 1981. Some effects of substrate roughness on wettability. *J. Mater. Sci.* 16(3): 714–32.
44. Shalz, M. L., Dalgleish, B. J., Tomsia, A. P., and Glaeser, A. M. 1993. Ceramic joining. I. Partial transient liquid-phase bonding of alumina via  $\text{Cu}/\text{Pt}$  interlayers. *J. Mater. Sci.* 28(6): 1673–84.
45. Shalz, M. L., Dalgleish, B. J., Tomsia, A. P., and Glaeser, A. M. 1994. Ceramic joining II Partial transient liquid-phase bonding of alumina via  $\text{Cu}/\text{Ni}/\text{Cu}$  multilayer interlayers. *J. Mater. Sci.* 29(12): 3200–8.
46. McKeown, J. T. 2003. Processing and characterization of alumina/niobium inter-

faces produced via liquid-film-assisted joining. M.S. thesis. Berkeley, Calif.: University of California.

47. McKeown, J. T., Sugar, J. D., Gronsky, R., and Glaeser, A. M. 2004. Niobium silicide formation at alumina-niobium interfaces processed via liquid-film-assisted joining. Unpublished research.

48. Derby, B., and Wallach, E. R. 1982. Theoretical model for diffusion bonding. *Met. Sci.* 16(1): 49–56.

49. Derby, B., and Wallach, E. R. 1984. Diffusion bonding: Development of theoretical model. *Met. Sci.* 18(9): 427–31.

50. Sugar, J. D. 2003. Mechanisms of metallic-interlayer/ceramic interface microstructure development during liquid-film-assisted bonding. M.S. thesis. Berkeley, Calif.: University of California.

51. Saiz, E., Tomsia, A. P., and Cannon, R. M. 1999. Energetics and atomic transport at liquid metal/ $Al_2O_3$  interfaces. *Acta Mater. (USA)* 47(15): 4209–20.

52. Dauskardt, R. H., Lane, M., Ma, Q., and Krishna, N. 1998. Adhesion and debonding of multilayer thin film structures. *Eng. Fract. Mech.* 61(1): 141–62.

53. Wenzel, R. N. 1936. Resistance of solid surfaces to wetting by water. *Ind. Eng. Chem.* 28(8): 988–94.

54. Shuttleworth, R., and Bailey, G. L. J. 1948. The spreading of a liquid over a rough solid. *Disc. Farad. Soc.* 3: 16–22.

55. Nicholas, M. G., Crispin, R. M., and Ford, D. A. 1984. Some effects of surface texture on melt-mold interactions during investment casting. *Proc. Brit. Ceram. Soc.* 34: 163–72.

## Appendix

Surface roughness can impact the wetting characteristics of the surface and liquid redistribution. A number of variables have been defined to characterize the surface roughness including  $R_a$  the average

deviation in surface height,  $\lambda_a$  the average distance between peaks of surface features,  $r$  the roughness parameter, and  $\alpha_a$  the average slope of surface features. Values of these parameters are given in Table 1, and some are used in the discussion. A brief summary of these parameters and their significance is provided here.

Wenzel (Ref. 53) proposed that an increase in surface area of a roughened plane causes a change in contact angle given by

$$\cos\theta_R/\cos\theta_0 = r \quad (1)$$

where  $\theta_R$  and  $\theta_0$  are the contact angles of sessile drops on, respectively, rough and smooth horizontal surfaces and  $r$  is the roughness factor, equal to the ratio of the true area to the apparent (projected) area. Asperities on a rough surface can act as barriers to liquid flow, which can significantly affect the contact angle predicted by the Wenzel relation. Shuttleworth and Bailey (Ref. 54) developed the following relation:

$$\theta_R = \theta_0 + \alpha_m \quad (2)$$

where the angle  $\alpha_m$  represents the maximum inclination that surface features make with the average plane of the surface. While the Wenzel model does not account for hysteresis (a difference in contact angles between advancing and receding liquid fronts), Shuttleworth and Bailey's analysis showed that  $\alpha_m$  could be positive or negative (and therefore  $\theta_R$  greater or less than  $\theta_0$ ) depending on whether the liquid front was advancing or receding. Minimization of the surface energy of the drop led to the conclusion that

an advancing front comes to rest on a descending slope ( $\alpha_m$  positive) and a receding front comes to rest on an ascending slope ( $\alpha_m$  negative).

Hitchcock et al. (Ref. 43) and Nicholas et al. (Ref. 55) investigated the wetting behavior of various liquid metals on ceramic surfaces. The irregularity of the ceramic surfaces made it difficult to derive values of  $r$  and  $\alpha_m$  using profilometry. Using the statistical parameters  $R_a$ , the average deviation in height of random points on the ceramic surface from a line drawn such that the cross-sectional areas of asperities above and grooves below are equal, and  $\lambda_a$ , the average distance between peaks of surface features, values of the roughness factor,  $r$ , and the average slope of surface features,  $\alpha_a$ , were obtained from the following expressions:

$$r = 1 + K_1(R_a/\lambda_a)^2 \quad (3)$$

$$\alpha_a = \tan^{-1}K_2(R_a/\lambda_a) \quad (4)$$

where  $K_1$  and  $K_2$  are arithmetic factors dependent on surface topography equal to about 50 and 9, respectively. For values of  $(R_a/\lambda_a)$  up to about 0.06,  $\tan \alpha_a$  is a nearly linear function of  $\alpha_a$  and Equation 4 can be simplified to

$$\alpha_a \cong 500(R_a/\lambda_a) \quad (5)$$

when  $\alpha_a$  is expressed in degrees. A linear relationship was observed between  $\theta_R$  and  $\alpha_a$ :

$$\theta_R = \theta_0 + \alpha_a \quad (6)$$

This relationship is in agreement with the analysis of Shuttleworth and Bailey.

## CAN WE TALK?

The *Welding Journal* staff encourages an exchange of ideas with you, our readers. If you'd like to ask a question, share an idea or voice an opinion, you can call, write, e-mail or fax. Staff e-mail addresses are listed below, along with a guide to help you interact with the right person.

### Publisher/Editor

Andrew Cullison  
cullison@aws.org, Extension 249  
Article Submissions

### Senior Editor

Mary Ruth Johnsen  
mjohansen@aws.org, Extension 238  
Feature Articles

### Associate Editor

Howard Woodward  
woodward@aws.org, Extension 244  
Society News, Personnel

### Assistant Editor

Kristin Campbell  
kcampbell@aws.org, Extension 257  
New Products, New Literature

### Production Editor

Zaida Chavez  
zaida@aws.org, Extension 265  
Design and Production

### Advertising Sales Director

Rob Saltzstein  
salty@aws.org, Extension 243  
Advertising Sales

### Advertising Production Coordinator

Frank Wilson  
fwilson@aws.org, Extension 465  
Advertising Production

### Advertising Sales & Promotion Coordinator

Lea Garrigan  
garrigan@aws.org, Extension 220  
Production and Promotion

### Peer Review Coordinator

Doreen Kubish  
doreen@aws.org, Extension 275  
Peer Review of Research Papers

Welding Journal Dept.  
550 N.W. LeJeune Rd.  
Miami, FL 33126  
(800) 443-9353  
FAX (305) 443-7404